Earthq Eng & Eng Vib (2014) 13: 203-214 **DOI**: 10.1007/s11803-014-0224-2

Uplift mechanism for a shallow-buried structure in liquefiable sand subjected to seismic load: centrifuge model test and DEM modeling

Zhou Jian[1†], Wang Zihan[2‡], Chen Xiaoliang[3§] and Zhang Jiao[4*]

1. *Department of Geotechnical Engineering, Tongji University, Shanghai 200092, China*
2. *School of Civil Engineering, Hebei University of Technology, Tianjin 300401, China*
3. *Hangzhou Municipal Construction Group Co., LTD, Hangzhou 310006, China*
4. *School of Civil Engineering and Transportation, Shanghai Technical College of Urban Management, Shanghai 200432, China*

Abstract: Based on a centrifuge model test and distinct element method (DEM), this study provides new insights into the uplift response of a shallow-buried structure and the liquefaction mechanism for saturated sand around the structure under seismic action. In the centrifuge test, a high-speed microscopic camera was installed in the structure model, by which the movements of particles around the structure were monitored. Then, a two-dimensional digital image processing technology was used to analyze the microstructure of saturated sand during the shaking event. Herein, a numerical simulation of the centrifuge experiment was conducted using a two-phase (solid and fluid) fully coupled distinct element code. This code incorporates a particle-fluid coupling model by means of a "fixed coarse-grid" fluid scheme in PFC3D (Particle Flow Code in Three Dimensions), with the modeling parameters partially calibrated based on earlier studies. The physical and numerical models both indicate the uplifts of the shallow-buried structure and the sharp rise in excess pore pressure. The corresponding micro-scale responses and explanations are provided. Overall, the uplift response of an underground structure and the occurrence of liquefaction in saturated sand are predicted successfully by DEM modeling. However, the dynamic responses during the shaking cannot be modeled accurately due to the restricted computer power.

Keywords: centrifuge modeling; underground structure; liquefaction; distinct element method; saturated sand

1 Introduction

Displacements arising from seismic liquefaction can be very large and are a major concern for underground structures located in regions of moderate to high seismicity. Liquefaction is caused by high excess pore-water pressures resulting from the tendency for granular soils to compact when subjected to cyclic loading. Metro stations and underground structures are vulnerable to damage caused by floatation or sinkage as the soil liquefies during an earthquake. The rational design for remediation requires a reliable prediction of soil-structure response during the design earthquake (Fiegel and Kutter, 1994; Yang *et al*., 2004).

As an alternative to actual earthquakes, dynamic centrifuge modeling can be used to study the effects of shaking on soil, and in particular, failure mechanism involving liquefaction. A rich body of centrifuge tests has been dedicated to sand liquefaction and soil-structure interaction (Byrne *et al*., 2004). However, the experimental models are placed in the environment with high centrifugal acceleration. The homogeneity of the soil, the boundary effect and the saturation degree should also be taken into account (Turan *et al*., 2009). All the uncertainty can cause problems for geotechnical engineers when researching liquefaction mechanisms, and also makes it very difficult to evaluate the results.

The numerical method, involving dynamic finite element or finite difference analyses using effective stress procedures coupled with fluid flow predictions, has been widely used for estimation of liquefaction potential for decades (Liu and Song, 2005). If some centrifuge tests are finished first, the experimental results can be repurposed through numerical simulation to obtain a feasible numerical model which can be used to predict the dynamic responses under other excitation conditions. Nevertheless, traditional methods are based on continuous medium theory instead of distinct element method (DEM) (Cundall and Strack, 1979). The DEM assumes basic constitutive laws at interparticle contacts and provides a macro/micro response of the particle assemblage due to incremental loading (Thornton, 2000). However, there is little evidence in micro-scale from centrifuge model tests to verify the results from DEM (Sitharam, 2003; Shamy and Zeghal, 2007).

Correspondence to: Wang Zihan, School of Civil Engineering, Hebei University of Technology, Tianjin 300401, China
Tel: +86-22-60435983
E-mail: wangzihan1984@163.com
[†]Professor; [‡]Lecturer; [§]Engineer; [*]Associate Professor

Supported by: National Natural Science Foundation of China under Grant Nos. 41272296 and 51208294
Received December 3, 2012; **Accepted** May 25, 2013

The main objective of this study is to provide a new perspective which unifies the liquefaction mechanism in both the macro-scale and micro-scale, and to promote a coherent understanding of soil mechanics under the interaction between the soil particles, the liquid and the underground structure. For this aim, a dynamic centrifuge model test on saturated sand deposits with a shallow-buried structure model was performed. A high-speed microscopic camera was installed in the structure model, by which the movements of particles and the interaction between fluid and particles were monitored during testing. Then, a numerical simulation of the centrifuge experiment was conducted by using the "fixed coarse-grid" fluid scheme in PFC3D. The occurrence of liquefaction in saturated sand is portrayed through the DEM modeling. The corresponding micro-scale responses and explanations are provided.

2 Centrifuge testing program

2.1 Apparatus and materials

A centrifuge model test on saturated sand deposits with a shallow buried structure model was performed on the geotechnical centrifuge at Tongji University in China at a centrifugal acceleration of 50 g. The 3 m radius geotechnical centrifuge is equipped with a servohydrauic actuator (shaker) that is capable of reproducing realistic scaled earthquake time histories and spectra. The time history was a simulated Kobe earthquake in Japan with the motion scaled to produce a peak base acceleration of about 0.32 g. Pore pressure transducers, accelerometers, and linear variable differential transformers (LVDTs) were used to measure soil response, and the model test was performed using a 50-cm-long, 40-cm-wide, and 56-cm-high laminar model box (Fig. 1). A clean, uniformly graded medium sand (Fujian standard sand in China) with a coefficient of uniformity (C_u) of 1.9 was used. The mean grain size (d_{50}), minimum void ratio (e_{min}), and maximum void ratio (e_{max}) are 0.35 mm, 0.519, and 0.848, respectively. The medium sand was overlaid by a layer of relatively impermeable saturated clay (5 cm in thickness), which tended to restrict the escape of pore water produced by the settlement of an underlying liquefiable sand layer. With high strength aviation aluminum-alloy as the main material, the structure model is a cube of 21.4 cm × 21.4 cm × 21.4 cm, and the mass is 16.1 kg. A high-speed microscopic camera was installed in the structure model, by which the movements of particles around the structure model were recorded through the tempered glass (0.8 cm in thickness) installed on the shooting side (Fig. 2). The shooting side is parallel to the direction of shaking. The structure model is able to operate properly and steadily at a centrifugal acceleration of 50 g without deformation and leakage.

The scaling laws for dynamic centrifuge modeling are described in some detail by Schofield (1981) and Kutter (1992). The main principle in centrifuge modeling is that a $1/N$ scale model subject to a gravitational acceleration of N g will feel the same stresses as the prototype. A known conflict exists between the time scale factors used for dynamic shaking, $1/N$, and pore-water pressure dissipation, $1/N^2$. This conflict can be resolved by changing the pore-fluid viscosity or by recognizing that the model soils actually simulate prototype soils with an absolute permeability N times greater (Tan and Scott, 1985). Scaling permeability, k, in this second manner allows for $1/N$ scaling of time during both dynamic shaking and pore-water pressure dissipation. While the research emphasis has been on the

Fig. 1 Laminar model box

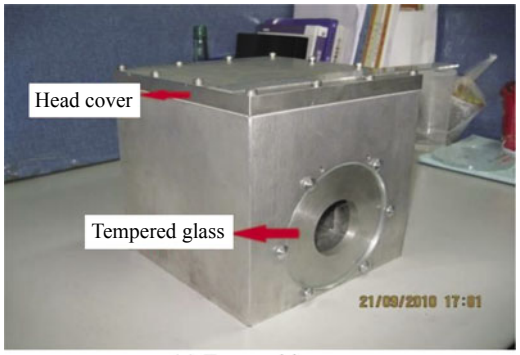

(a) External image

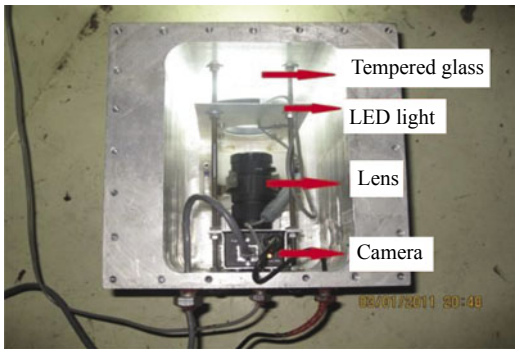

(b) Internal image

Fig. 2 Underground structure model

liquefaction mechanism, the time scale is not the main influence factor (Su, 2005). Therefore, it is reasonable to choose water as the pore fluid in the present study. In addition, more clear images could be obtained by the microscopic camera in this way.

2.2 Model construction

The centrifuge test was designed to model a level prototype ground surface. In order to simulate the natural sedimentary characteristics of a sand foundation in the southeast coast of China, the saturated sand was pluviated under the water surface through a screen. Before the centrifuge model test, the medium sand was immersed in water for one week. The model box was first flooded with deaired water of 20 cm in depth when making the saturated sample. The immersed sand was then scooped out and put into the screen, which was placed under the water in the model box. After that, the sand in the screen was agitated lightly by a flat plexiglass tool so that the sand particles were able to pass through the screen aperture and sink slowly into the water. These steps were repeated until the sand deposited to a specified height. Then, the excess water above the sedimentary surface was drawn off with a catheter. Finally, the saturated sand deposits were overlaid by a layer of relatively impermeable saturated clay (5 cm in thickness). The relative density (D_r) of the prepared sand is about 40%. Pore pressure transducers, accelerometers, displacement sensors and the structure model were installed at the specified positions when the sand deposited to the corresponding height.

Configuration for the centrifuge test is shown with model dimensions in Fig. 3. The centrifuge model simulated saturated sand deposits with the shallow buried structure model. In the model test, the sand layer, in model terms, was 45 cm thick. The boundary effects during shaking were expected to be small due to the use of the laminar model box.

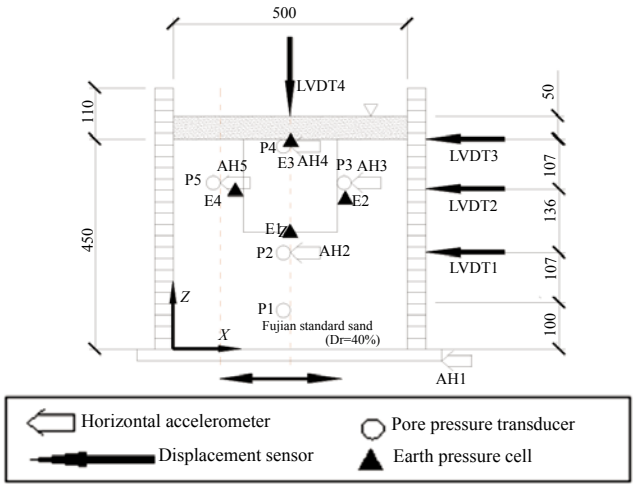

Fig. 3 Centrifuge model configuration (unit: mm)

3 Numerical modeling procedures

3.1 Particle flow code

In the past few decades, the DEM has been proven to be a very useful tool in soil mechanics, especially for granular mechanics (Thornton, 2000). PFC3D (Particle Flow Code in Three Dimensions; Itasca Consulting Group, Minneapolis, USA), a special DEM code, is based on spherical elements and the fundamental laws of contact physics. Thus, it is ideal to simulate the mechanical behavior of granular materials (Cundall and Strack, 1979). However, the main limitation of DEM is the computational requirement. Despite increased computing power, the number of particles that can be reasonably simulated is still significantly limited. In this study, a moderate enlargement of the diameters of soil particles is adopted to reduce the number of particles. Meanwhile, the ratio of maximum grain size to minimum grain size should be regulated so that the properties of specimen are close to those in the centrifuge test.

PFC3D elements can also be bonded to describe cohesive soils and structures. A "fixed coarse-grid" fluid scheme is implemented in PFC3D for particle-fluid coupling simulations (Shimizu, 2004). This scheme solves the continuity and Navier-Stokes equations for incompressible fluid flow numerically in an Eulerian Cartesian coordinate system, and then derives the pressure and fluid velocity for each fixed grid (or cell) by including the influence of particles, and the corresponding porosity, within each cell. The code has been successfully applied to various geotechnical problems.

3.2 Distinct element model

The numerical model built by PFC3D is exhibited in Fig. 4. The original code already provides spherical elements suitable for most analyses. However, there is a great difference in particle shape between the spheres and sand grains. The generalized non-spherical particles were therefore developed and incorporated into the program by Shi (2007). The sandy soil in the analyses was modeled using these non-spherical particles. The way to make a non-spherical shape is by using clump logic (Itasca, 2005). Figure 4(a) shows the creation of a clump with pair-particles. A compacted assembly of spherical particles was first created. Each particle was then converted to a clump with the same volume and weight as the original spherical particle. The aspect ratio of the clumps was 1:1.5.

The 3D and cross-sectional views of the numerical model are shown in Fig. 4(b) and Fig. 4(c), respectively. The sand layer, clay layer, and underground structure have the same size as their counterparts in the centrifuge model. The fixed fluid cells are shown in Fig. 4(d). In order for the fluid cells to be seen straight, the soil and structure are not plotted in Fig. 4(d). 8000 (20 × 20 × 20: length × width × height) fluid cells were created in the

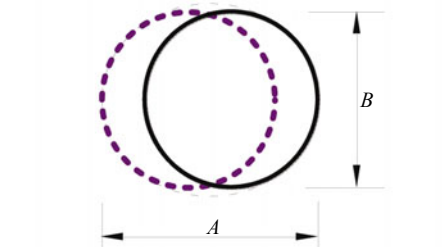

(a) Structure of non-spherical particle

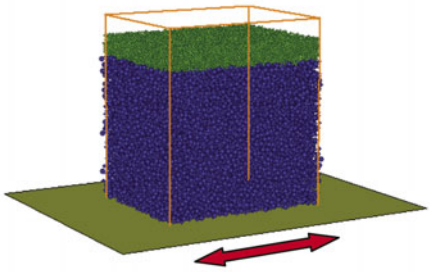

(b) 3D view of model

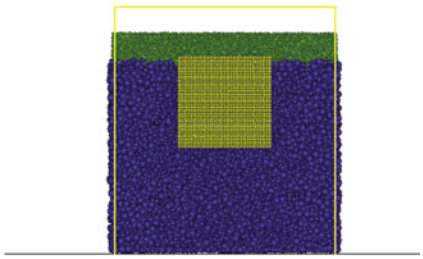

(c) Cross-sectional view of model

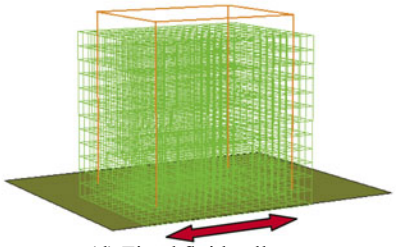

(d) Fixed fluid cells

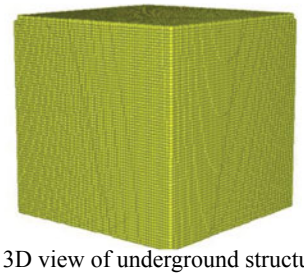

(e) 3D view of underground structure

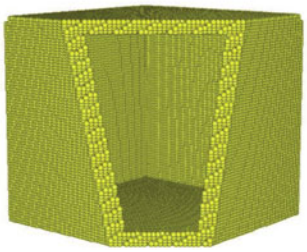

(f) Cross-sectional view of underground structure

Fig. 4 Numerical model built by PFC3D

rectangular space, which covered the model.

The 3D and cross-sectional views of the underground structure are shown in Fig. 4(e) and Fig. 4(f), respectively. The structure model was composed of a series of regularly arranged spherical particles joined by parallel bonds. By setting all bond strengths to a high value (5×10^{20} in this case), the entire structure remained intact during and after the shaking event. The mass and size of the structure model were identical with those in the centrifuge model.

3.3 Boundary conditions

For the solid phase, a rigid finite wall was used as the bottom boundary. Dynamic input was applied to the base of the model by way of a velocity history at an acceleration of 50 g, which was identical with that in the centrifuge test. To prevent the reflection of propagating waves back into the model, periodic boundaries were used to minimize the problem (Benyoussef *et al*., 1999). The periodic boundaries were specified at the lateral boundaries, by which particles existing at one vertical boundary appeared at the opposite boundary after crossing the periodic boundary.

For the fluid phase, the underground water level was assumed to locate at the ground surface. A zero pressure boundary was specified at the top of the model. The slip boundaries, in which the fluid velocity parallel to the boundary was non-zero at the boundary, were specified for the other boundaries.

In the physical test, due to a limited size of the model box and the consideration of microscopic camera in the structure model, the distance between the lateral side of the model box and the structure model had to be confined to a relatively small space. Although there is a boundary effect, the uplift mechanism for the structure model observed in the test is correct. For comparison, the apparent sizes and locations of the model box and structure in the numerical model are identical with those in the physical model.

3.4 Choice of parameters

Since the micro material parameters cannot be defined in a direct manner, a series of simulated triaxial tests and permeability tests have to be conducted during a multi-stage iterative calibration process, so that the relationship of these micro parameters to the general mechanical indices in the soil can be determined. The corresponding parameters should then be further adjusted in the simulation of the centrifuge test containing the same granular material as the sample. In this way, the adjusting efficiency can be greatly improved (Shimizu, 2004; Shi, 2007).

According to previous research results (Shi, 2007; Zhou, 2010), the micro parameters of the sand layer introduced in the nonlinear contact model are selected by comparing the experimental results with the numerical ones. Parallel bonds are used to approximate

Table 1 Soil and underground structure parameters

Sand layer		Clay layer		Underground structure	
Diameter (mm)	4-10	Diameter (mm)	2–4	Diameter (mm)	3.06
Density (kg/m^3)	2650	Density (kg/m^3)	2650	Density (kg/m^3)	1170
Shear modulus (MPa)	850	Normal stiffness (kPa/m)	1000	Normal stiffness (MPa/m)	500
Poisson's ratio	0.25	Shear stiffness (kPa/m)	1000	Shear stiffness (MPa/m)	500
Friction coefficient	0.5	Normal strength (GPa)	10	Normal strength (Pa)	5.0×10^{20}
Porosity	0.42	Shear strength (GPa)	10	Shear strength (Pa)	5.0×10^{20}
		Friction coefficient	0.5	Friction coefficient	0.5
		Porosity	0.3		

Table 2 Wall and fluid parameters

Wall		Fluid	
Normal stiffness (MN/m)	10	Density (kg/m^3)	1000
Shear stiffness (MN/m)	10	Viscosity (Pa.s)	9.21
Friction coefficient	0.5		

the physical behaviors of the clay layer and underground structure. The micro material parameters of this simulation are listed in Table 1 and Table 2. The range of the particle size of sand and clay layers is 4-10 mm and 2-4 mm, respectively.

As reported by Ishihara (1996), the damping of soil at small confining pressure is difficult to simulate. At the same time, the viscous effect of the pore fluid also incorporates damping. In PFC, the local damping is provided and damping is frequency-independent (Itasca, 2005). Therefore, a relatively smaller value of 5% is set as the local damping coefficient in this simulation.

4 Results analyses

The uplift displacement of the underground structure, the acceleration responses, the build-up of excess pore pressure, as well as the transition of the microstructure during shaking were investigated in order to gain a comprehensive insight into the seismic behavior of the liquefiable soil-structure interaction system.

4.1 Uplift response of underground structure

There were significant uplifts of the structure model observed in both physical and numerical models (Figs. 5 and 6) due to the accumulation of pore pressure at the bottom of the structure model. The photograph of the centrifuge test in Fig. 5 shows that the top of the underground structure emerged on the surface of the clay layer after shaking. The sand and clay particles are carried to the model surface through the cracks and deposit over the top of the black clay layer.

Fig. 5 Uplift of structure model in centrifuge test

Figure 6 depicts the computed deformed configurations at different stages during the shaking event. In order for the uplift response of the underground structure to be seen straight, only the cross-sectional views of the numerical model are plotted in Fig. 6. Model time values in the plots have been multiplied by N to represent a prototype in dynamic terms. That is, the seismic duration time is 40 s. During the liquefaction process, the uplift of the underground structure was very obvious from the figures. The middle part of the clay layer was pushed up by the structure model. The soil near the side of the underground structure was pushed into the open space, which situated under the structure.

Figure 7 shows the measured and computed uplift displacement time histories. Both displacement and time values have been scaled to represent prototype values. In the physical model, the uplift displacement measured by LVDT4 located at the center of the surface of the clay is shown in Fig. 7(a). The location of each transducer is shown in Fig. 3. The uplift displacement developed rapidly during the 5–25 s shaking phase and eventually reached a peak. After that, the displacement remained almost unchanged. The maximum uplift displacement recorded was approximately 60.81 cm. Numerically, the uplift displacement time history was very similar to that in the physical model (Fig. 7(b)). The differences were that the computed uplift displacement was more stable at the earlier stage of shaking and the peak time delayed about 5 s corresponding to the recorded data. Eventually, the maximum uplift displacement computed was approximately 61.5 cm. In other words, the predicted uplift history was surprisingly in agreement with the experiment results.

4.2 Acceleration responses

The recorded and computed acceleration time histories are presented in prototype terms in Fig. 8. The

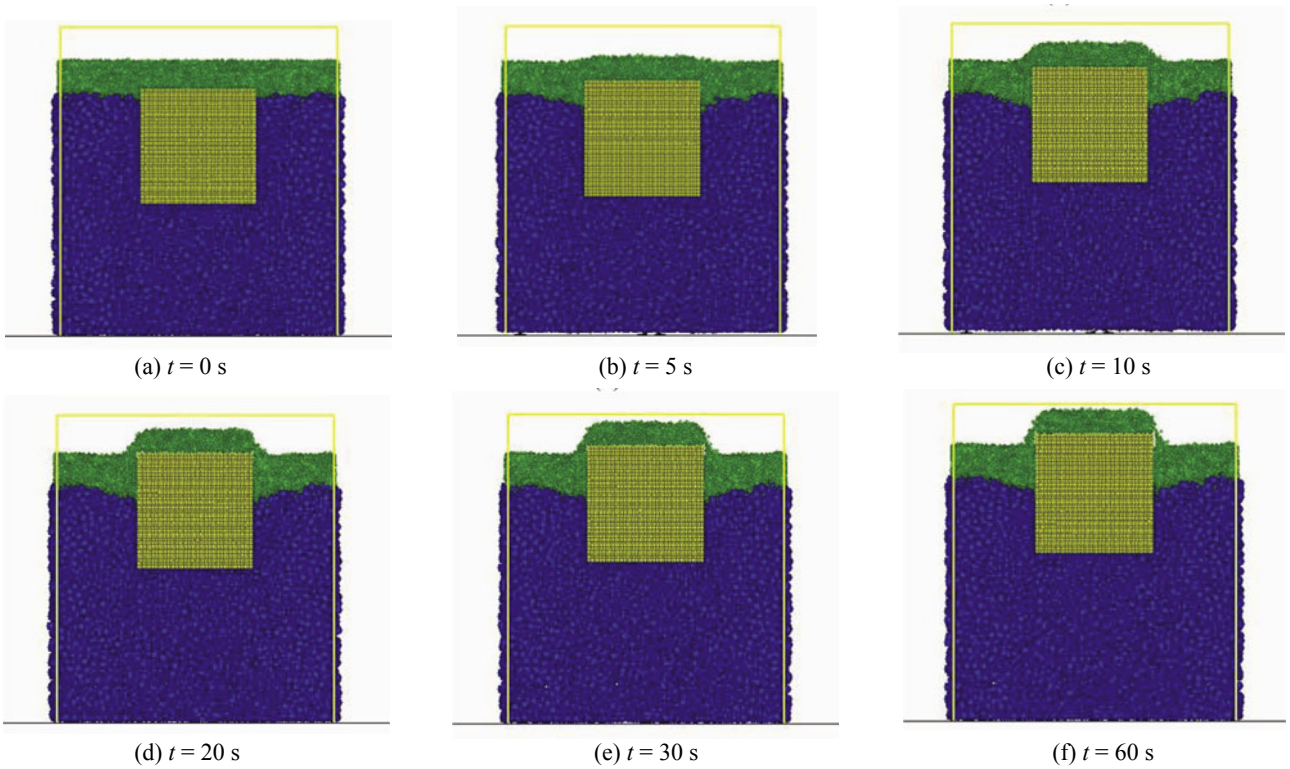

(a) t = 0 s (b) t = 5 s (c) t = 10 s

(d) t = 20 s (e) t = 30 s (f) t = 60 s

Fig. 6 Computed deformed configurations

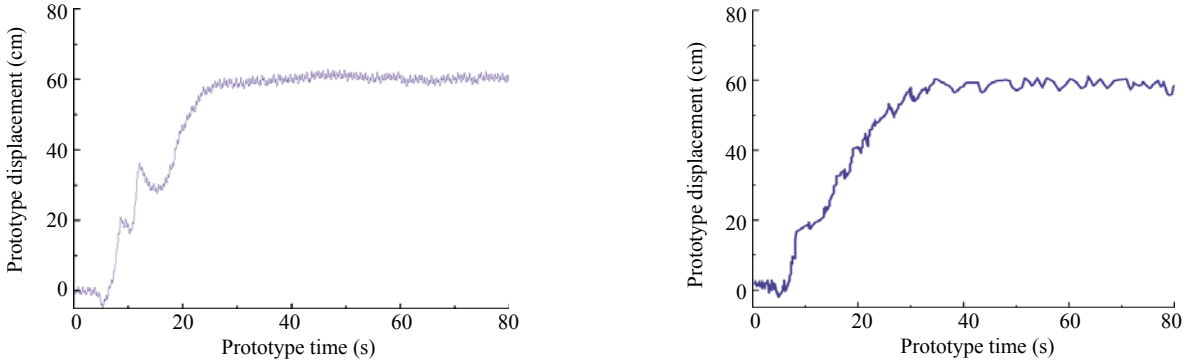

(a) Measured uplift history (b) Computed uplift history

Fig. 7 Uplift displacement time histories

bottom acceleration (AH1) represents the input motion at the base. The results are not presented. The peak acceleration recorded by AH2-AH5 was 0.179 g, 0.085 g, 0.051 g, and 0.078 g, respectively. The acceleration at the sand-clay interface (AH4) was maintained at about zero after 12 s of shaking (Fig. 8(c)). It can be inferred that, at this point, the sand near the sand-clay interface was fully liquefied. AH3 and AH5 were located at the same level. AH3 was placed close to the structure model so that the acceleration amplitude was significantly greater than that recorded by AH5. Meanwhile, the higher frequency components in the acceleration were recorded by AH3 (Fig. 8(e)). In addition, some asymmetric acceleration spikes were exhibited experimentally.

In the numerical model, the acceleration time histories at the corresponding positions where the accelerators (AH2-AH5) are located in the centrifuge test are also depicted in Fig. 8. For comparison, these positions are also named as AH2-AH5. The computed peak acceleration at AH2-AH5 was 0.21 g, 0.09 g, 0.05 g, and 0.08 g, respectively. It can be seen that, due to the enlargement of the size of the particles, the numerical model somewhat over-predicted the peak acceleration, especially for the sand at deep depth (AH2). In addition, when liquefaction occurred, there were still certain accelerations in the shallow sand layer (Figs. 8(b) and (d)). Despite the fact that the numerical results were somehow imperfect, the acceleration responses were predicted reasonably well.

4.3 Excess pore pressure in the soils

Figure 9 depicts the recorded and computed excess pore pressure time histories at different depths. The excess pore pressure histories at the same level (P3 and P5) showed a consistent performance in both the

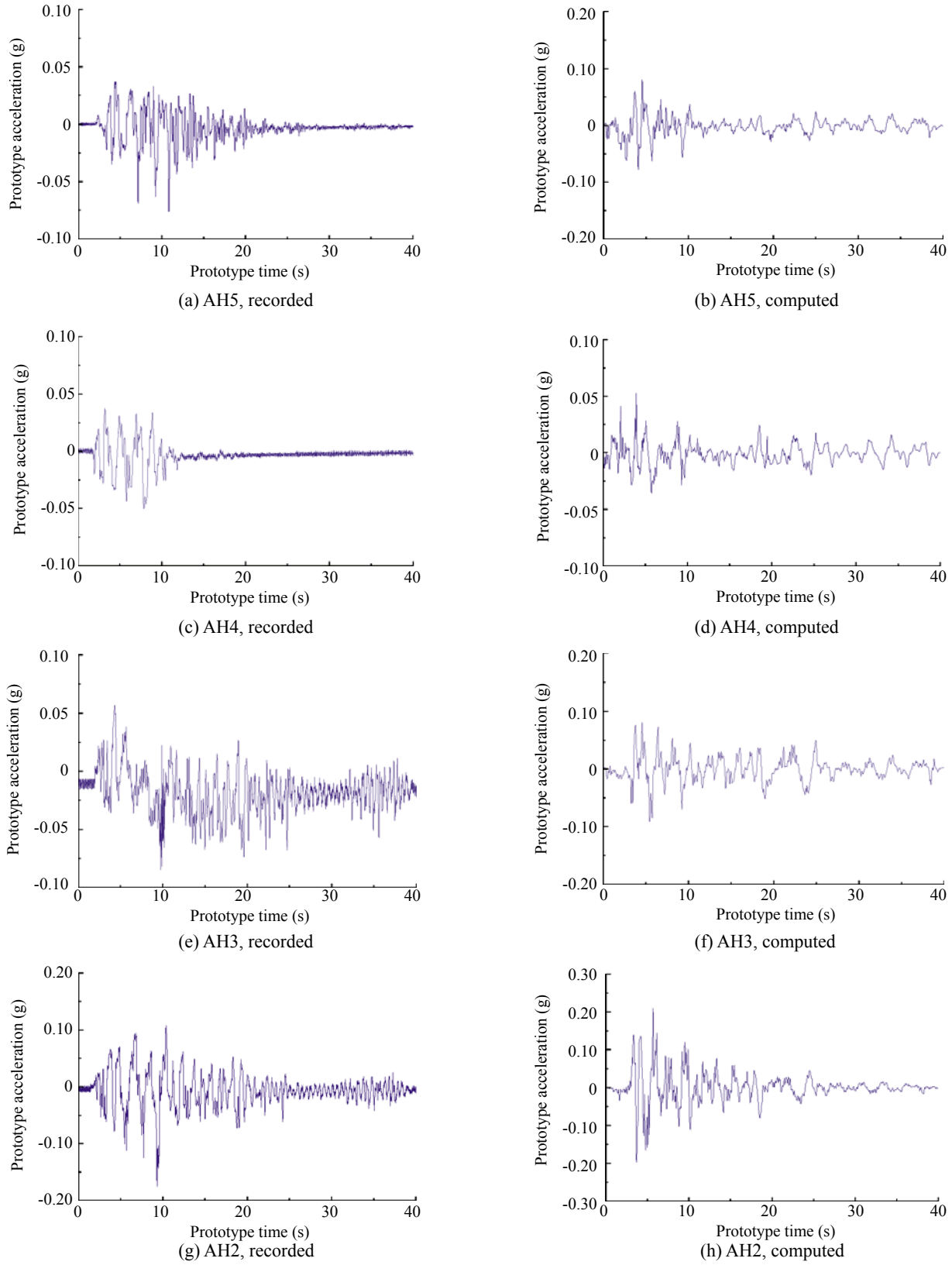

Fig. 8 Horizontal acceleration time histories

physical and numerical models. The results about P5 are not presented here. Initial measurements have been used to calculate an initial overburden pressure value, σ'_{v0}; the ratio of excess pore pressure (u) to this value is defined as the excess pore pressure ratio. The recorded pore pressures followed a similar trend with the variation of measured locations. Pore pressures rose rapidly during the 2–5 s shaking phase; then, after the period of fluctuation on the peak plateau, pore pressures began to dissipate at about t = 10 s. Eventually, a little residual

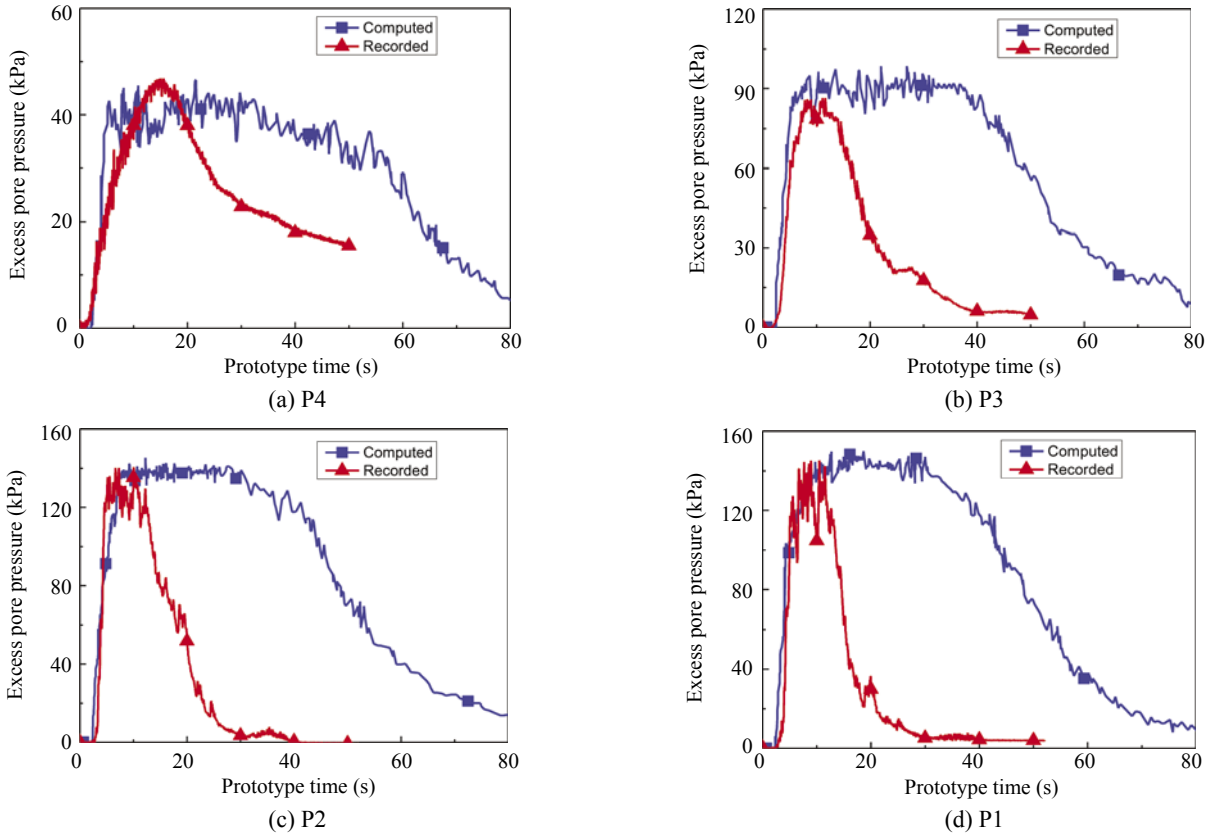

Fig. 9 Excess pore pressure time histories

excess pore pressures was measured. The maximum excess pore pressure recorded by P1-P4 was 145.47 kPa, 140.62 kPa, 86.33 kPa, and 46.86 kPa, respectively; the corresponding excess pore pressure ratio was 0.83, 0.94, 1.03, and 1.03, respectively. It can be inferred that the sand deposits near the side of the underground structure reached a condition of zero effective stress ($u/\sigma'_{v0} \approx$ 100%) and were entirely liquefied. Additionally, the pore pressure transducer at the sand-clay interface (P4) was penetrated into the clay layer during the shaking. The data recorded by P4 had little significance after the peak time.

After the experiment was over, the excess water above the clay surface was drawn off; and the soil was dug out of the model box. When the structure model was dug out, a water interlayer was observed under the bottom of it. Thus, it was observed that the pore pressure accumulated at the bottom of structure model during the shaking event.

For comparison, the corresponding positions where pore pressure transducers (P1-P4) were located in the centrifuge test were also named as P1-P4 in the numerical test. The computed maximum pore pressure at P1-P4 was 150.79 kPa, 145.62 kPa, 98.51 kPa, and 46.58 kPa, respectively, which showed a close match with the recorded counterparts. However, the computed results displayed a much longer peak plateau in every computed position. Excess pore pressures began to dissipate at about t = 30 s. In addition, there were still certain excess pore pressures at t = 80 s, however, the shaking stopped at t = 40 s. The dissipation rates were lower than in the centrifuge test.

On one hand, in the physical model, with the uplift of structure model, the upper clay layer began to crack. New drainage channels were gradually generated in this process, resulting in increases of permeability and dissipation rate of the pore pressure. The process was not simulated effectively in the numerical test, because the granular particles have to be applied to simulate clay layer, which is actually more like a continuous medium. On the other hand, in the numerical model, based on the mechanism for generation of pore pressure, any tiny movement of large particles can also cause a great change in pore pressure that is computed in the fluid cell (Shimizu, 2004). In the late period of simulation, although the shaking was remarkably weakened, the particles still present a trend of compacting, which leads to the continuous generation and a decreased dissipating rate of pore pressure. Better numerical results may be achieved by using even smaller particles whose sizes are closer to the sand and clay grains.

4.4 Micro-scale responses

In the experiment, a high-speed microscopic camera was installed in structure model, by which the movements of particles around the model were recorded (Fig. 10). Then, a quantitative analysis was conducted on the microstructure of saturated sand around structure model using 2D digital image processing software called

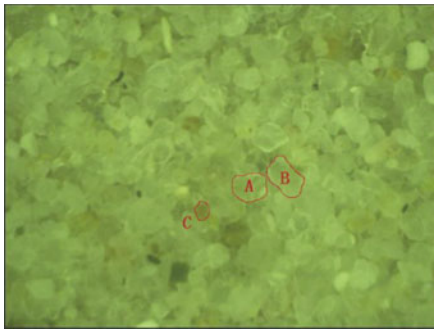

Fig. 10 2D digital image recorded by microscopic camera

GEODIP (developed independently, and was certified by China State Bureau of Copyrights with standard serial number of 2010SR019305). Based on digital image processing technology, the microstructure parameters of granular soils, such as the orientation of particle long axis, average coordination number, and porosity in 2D, can be easily obtained (Zhou *et al*., 2006).

The evolution of the orientation of particle long axis is shown in Fig. 11. The distributions of particle long axis were extracted at different stages during the shaking. At the start of shaking, the rose diagram indicated a preferred direction of particle long axis, which was close to the horizontal direction due to the natural sedimentary characteristics of sand deposits. Then, with the rose in pore pressure, the rose diagram favored uniform distribution at t = 5 s. At t = 10 s, the particles around the structure model had different orientations, where upward dissipation of pore pressure forced the particles to orient preferably to the vertical direction. Eventually, the sand began to deposit again after the shaking event. Therefore, the rose diagram had a slightly different distribution, with preferred angles of 40° and 140°.

2D average-coordination-number (average number of contacts per particle) time history is shown in Fig. 12. Note that a coordination number of 3.0 or higher is required for a stable 2D deposit of frictional particles (Edwards and Grinev, 2001). At the start of the shaking, the sand deposits around the structure model had a coordination number of 3.931. Thereafter, this number decreased suddenly to 1.301 at about t = 5 s. This was mainly because excess pore pressure ratio reached about 1.0; the sand particles separated suddenly at this point. After that, with the dissipation of pore pressure, the coordination number began to increase gradually after

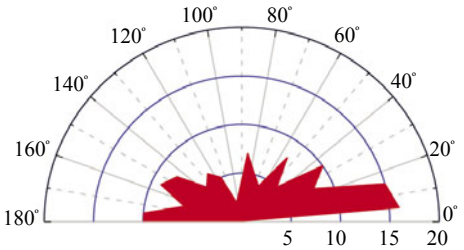

(a) t = 0 s

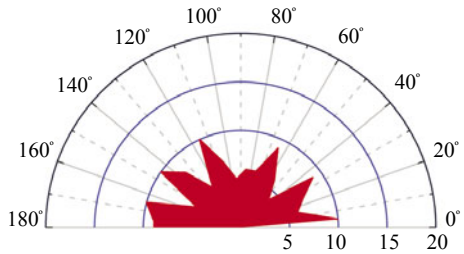

(b) t = 5 s

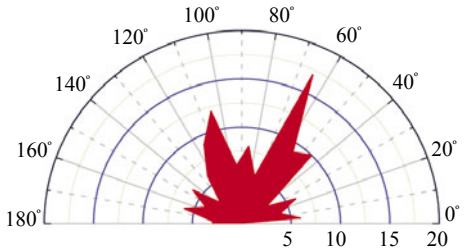

(c) t = 10 s

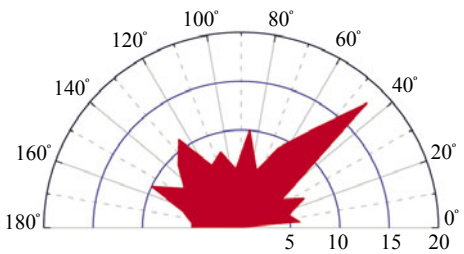

(d) t = 40 s

Fig. 11 Rose diagrams of particle long axis

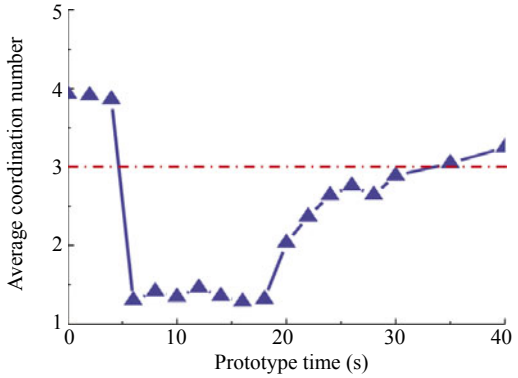

Fig. 12 2D average-coordination-number time history

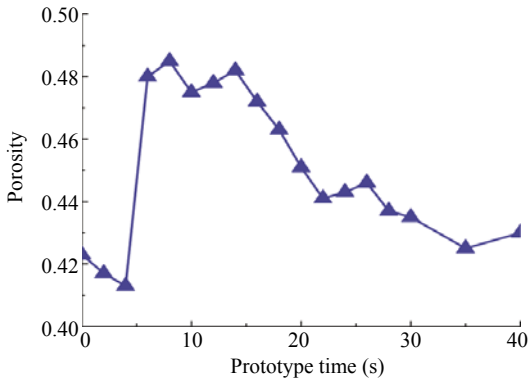

Fig. 13 2D porosity time history

18 s of shaking. Eventually, this number increased to a value above 3.0 after the shaking event.

The 2D porosity time history is shown in Fig. 13. Due to the effect of vibration densification, the porosity decreased in the first five seconds. Then, the porosity increased suddenly, corresponding to the sudden decrease in average coordination number. After that, with the deposition of sand particles, the porosity began to decrease gradually and eventually reached 0.43.

Numerically, the whole model can be monitored through the simulation procedure rather than the small area that was observed in the centrifuge test. Figure 14 depicts the computed particle velocity vectors at different stages during the shaking. Only the cross-sectional views are plotted in order to be seen straight. At the earlier stage of shaking, the particles in the lower part of the sand layer presented remarkable movements (Figs. 14(a) and (b)). At about t = 15 s, all the particles showed high velocities, which represented a complete break with the original stable state. After that, with the decrease in vibrant intensity, the particles around the structure were pushed into the space that situated

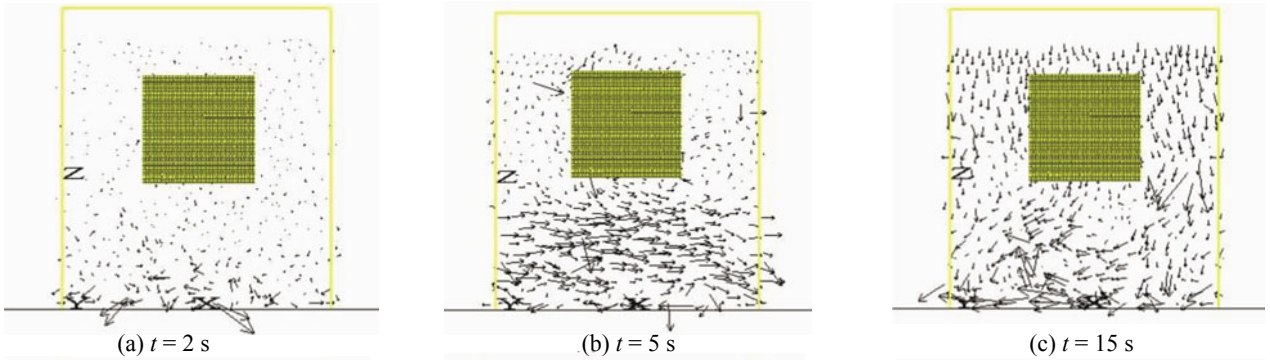

(a) t = 2 s (b) t = 5 s (c) t = 15 s

(d) t = 20 s (e) t = 30 s (f) t = 80 s

Fig. 14 Particle velocity vectors

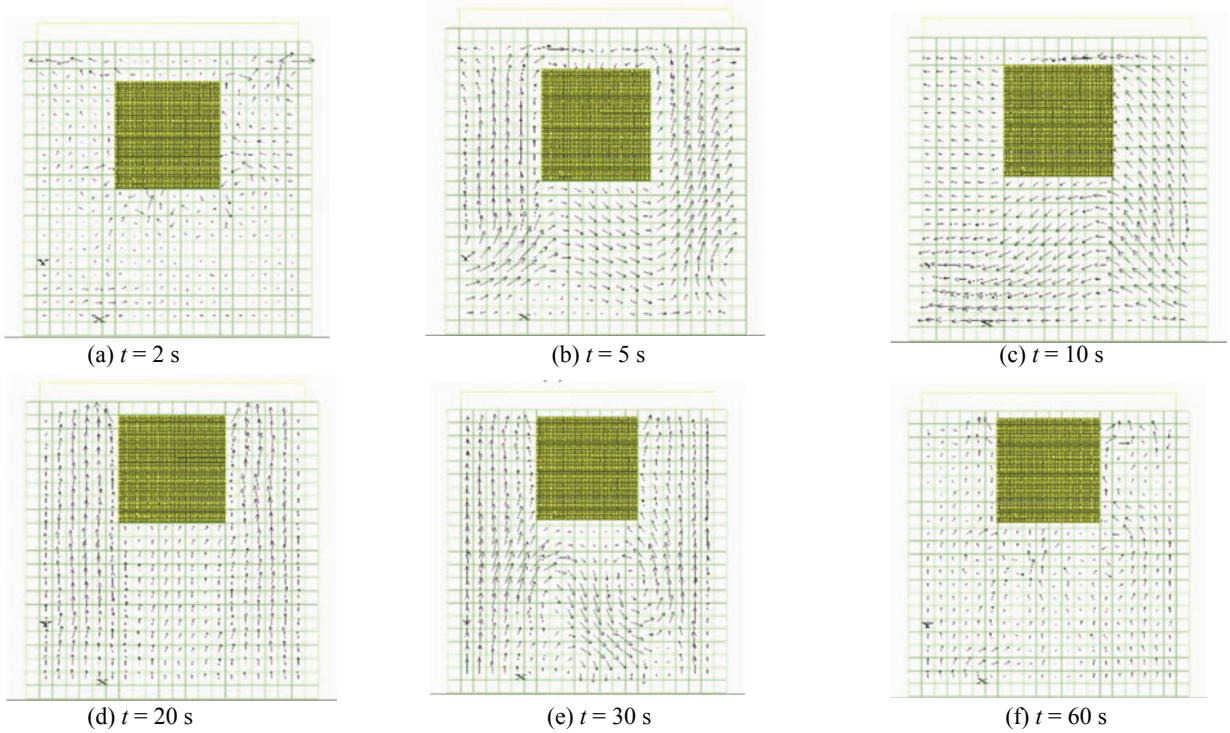

(a) t = 2 s (b) t = 5 s (c) t = 10 s

(d) t = 20 s (e) t = 30 s (f) t = 60 s

Fig. 15 Fluid velocity vectors

under the structure, and further promoted the uplift of the underground structure (Figs. 14(d) and (e)). After the shaking stopped, all the particles began to deposit again. The particle velocities under the structure bottom were slightly larger than the others (Fig. 14(f)).

Figure 15 depicts the cross-sectional views of the fluid velocity vectors at different stages during the shaking event. At the start of shaking, the fluid velocities appeared at first in the upper fluid cells (Fig. 15(a)). During the shaking, the fluid showed remarkable upward movements, which promoted the uplift of the structure model. The fluid velocities under the structure bottom changed the upward direction and rounded the underground structure (Figs. 15(b)–(e)). After the shaking was over, with continuous dissipation of pore pressure, some certain upward velocities remained in the fluid cells (Fig. 15(f)). In both the physical and numerical models, the micro-scale responses were in good agreement with the macro-scale behavior during the shaking event.

5 Concluding remarks

Based on centrifuge model testing and DEM modeling, this study provides a new perspective which unifies the liquefaction mechanism for saturated sand and uplift response of underground structures observed in macro and micro scales. The main conclusions can be described as follows.

Excess pore pressure in liquefiable soils rose rapidly during the initial stage of the earthquake, resulting in an upward movement of pore fluid. The upper soils first became liquefied, and the acceleration response suddenly experienced a sharp decline. The corresponding micro responses included: (a) a preferred vertical orientation of particle long axis; (b) a sudden decrease in coordination number; and (c) a sudden increase in porosity.

Due to liquefaction, a significant uplift of the shallow buried structure was observed during the shaking event. The major causes for uplift response were as follows: (a) an accumulation of pore pressure at the structure bottom; (b) a low overburden pressure on the top of the underground structure; (c) a decline in lateral confinement, which exerted on the sides of structure, as the soils around structure liquefied; and (d) an upward push exerted on the structure bottom, as the soils around structure moved to the space that was situated under the structure during shaking.

During shaking, the occurrence of liquefaction in saturated sand was predicted successfully by using the "fixed coarse-grid" fluid scheme in PFC3D. However, the dynamic responses during the liquefaction procedure cannot be modeled accurately, such as acceleration and excess pore pressure. In the future, with more rapid development in computer power, better numerical results may be achieved using smaller particles whose sizes are closer to sand grains.

With the development of urban underground space, liquefaction evaluation involving shallow buried structures should be given more attention than simple evaluation in the free field, as is the current practice.

Acknowledgment

The authors are grateful for the support from the National Natural Science Foundation of China under Grant Nos. 41272296 and 51208294.

References

Benyoussef A, Chakib H and Ez-Zahraouy H (1999), "A Simulation Study of an Asymmetric Exclusion Model with Open and Periodic Boundaries for Parallel Dynamics," *The European Physical Journal B - Condensed Matter and Complex Systems*, **8**(2): 275–280.

Byrne P, Park S, Beaty M *et al*. (2004), "Numerical Modeling of Liquefaction and Comparison with Centrifuge Tests," *Canadian Geotechnical Journal*, **41**(2): 193–211.

Cundall P and Strack O (1979), "A Discrete Numerical Model for Granular Assemblies," *Geotechnique*, **29**(1): 47–65.

Edwards S and Grinev D (2001), "Transmission of Stress in Granular Materials as a Problem of Statistical Mechanics," *Physica A: Statistical Mechanics and its Applications*, **302**(1-4): 162–186.

Fiegel G and Kutter B (1994), "Liquefaction Mechanism for Layered Soils," *Journal of Geotechnical Engineering*, **120**(4): 737–755.

Ishihara K (1996), *Soil Behavior in Earthquake Engineering*, Oxford University Press, NY, USA.

Itasca (2005), *PFC3D Particle Flow Code in Three Dimensions*, Itasca consulting group, Inc., Minneapolis, MN, USA.

Kutter B (1992), "Dynamic Centrifuge Modeling of Geotechnical Structures," *Transportation Research Record No. 1336*, Transportation Research Board, Washington D.C., pp. 24–30.

Liu Huabei and Song Erxiang (2005), "Seismic Response of Large Underground Structures in Liquefiable Soils Subjected to Horizontal and Vertical Earthquake Excitations," *Computers and Geotechnics*, **32**(4): 223–244.

Schofield A (1981), "Dynamic and Earthquake Geotechnical Centrifuge Modeling," *Proceeding of International Conference on Recent Advances in Geotechnical Earthquake Engineering and Soil Dynamics*, Vol. III, University of Missouri, Rolla, pp. 1081–1100.

Shamy U and Zeghal M (2007), "A Micro-mechanical Investigation of the Dynamic Response and Liquefaction

of Saturated Granular Soils," *Soil Dynamics and Earthquake Engineering*, **27**(8): 712–729.

Shi Danda (2007), "Micromechanical Simulations of Sand Behavior Under Monotonic and Cyclic Loading," *PhD Dissertation*, Tongji University, Shanghai, China. (in Chinese)

Shimizu Y (2004), "Fluid Coupling in PFC2D and PFC3D," *Proceedings of the 2nd International PFC Symposium in Numerical Modeling in Micromechanics*, Kyoto, Japan, pp. 281–287.

Sitharam T (2003), "Discrete Element Modelling of Cyclic Behaviour of Granular Materials," *Geotechnical and Geological Engineering*, **21**(4): 297–329.

Su Dong (2005), "Centrifuge Investigation on Response of Sand Deposit and Sand-pile System Under Multi-directional Earthquake Loading," *PhD Dissertation*, Hong Kong University of Science and Technology, Hong Kong.

Tan T and Scott R (1985), "Centrifuge Scaling Considerations for Fluid-particle Systems," *Geotechnique*, **35**(4): 461–470.

Thornton C (2000), "Numerical Simulation of Deviatoric Shear Deformation of Granular Media," *Geotechnique*, **50**(1): 43–53.

Turan A, Hinchberger S and El Naggar H (2009), "Design and Commissioning of a Laminar Soil Container for Use on Small Shaking Tables," *Soil Dynamics and Earthquake Engineering*, **29**(2): 404–414.

Yang Z, Elgamal A, Adalier K *et al*. (2004), "Earth Dam on Liquefiable Foundation and Remediation: Numerical Simulation of Centrifuge Experiments," *Journal of Engineering Mechanics*, **130**(10): 1168–1176.

Zhou Jian, Yu Rongchuan and Jia Mincai (2006), "Measurement of Microstructure Parameters for Granular Soil Model Using Digital Image Technology," *Chinese Journal of Geotechnical Engineering*, **28**(12): 2047–2052. (in Chinese)

Zhou Kaimin (2010), "Research on the Macro-meso Mechanism of Rainfall-induced Sandy Soil Flow," *PhD Dissertation*, Tongji University, Shanghai, China. (in Chinese)